# Surface electronic structure of Cr(001): Experiment and theory

O. Yu. Kolesnychenko, G. M. M. Heijnen, A. K. Zhuravlev, R. de Kort, M. I. Katsnelson,
A. I. Lichtenstein, and H. van Kempen
*Institute for Molecules and Materials, Radboud University of Nijmegen, Toernooiveld 1, NL-6525 ED Nijmegen, The Netherlands*
(Received 4 March 2005; revised manuscript received 1 June 2005; published 26 August 2005)

Low-temperature scanning tunneling microscopy and spectroscopy investigations of the atomically clean Cr(001) surface together with density functional and many-body calculations have been used to study the surface electronic structure. The Friedel oscillations near impurity atoms have been observed and explained within the Fermi surface analysis. A very narrow resonance at 26 meV above the Fermi level has been observed and the orbital character of corresponding state has been visualized. The experimental data together with many-body calculations give further evidence that the observed resonance is an orbital Kondo resonance formed by two degenerated $d_{xz}, d_{yz}$ surface states. This gives evidence of strong correlation effects on transition metal surfaces.

DOI: 10.1103/PhysRevB.72.085456 PACS number(s): 73.20.At, 68.37.Ef, 71.27.+a

## I. INTRODUCTION

In recent years a new class of electronic devices which utilize the fundamental principle that electrons carry not only charge but also spin, so-called "spintronics," has emerged. One of the fields of this rapidly growing spin electronics is based on electron tunneling. In magnetic materials, where spin-up and spin-down electron populations are unequal, a tunneling current should naturally be spin polarized. In this case, a magnetic field can be used to manipulate spin polarized current, providing an additional channel of information as well as an additional degree of freedom for designing novel devices.

Starting from the pioneering experiments by Giaever[1] and following the theoretical model by Bardeen[2] it has been recognized that solid state tunneling is dependent on the density of states sampled within a few coherence lengths of the electrode-barrier interface.[3–5] Although in tunnel junctions the insulating material can influence transport properties of such a device, the role of the surface density of states of metal electrodes remains very important. Keeping in mind that in recent years a large variety of insulating materials including some organic composites emerge, it becomes crucial to understand the fundamental properties of metal surfaces itself. Also electronic structure of the surfaces sometimes is characterized by essentially new features such as an "orbital Kondo resonance" found recently for the Cr(001) surface.[6] Even for such "classical" multilayer systems as $Co/Al_2O_3/Co$ with thin Cr interfacial layers it turned out that more complicated many-electron phenomena originating from metal surface themselves are determining the tunneling of this system.[7] That is why in recent years surface science has witnessed intense research on the surface electronic properties of ferromagnetic and antiferromagnetic metals. Since the growth mode depends also on the surface electronic structure, it become the key feature to know and to control in order to construct new "spintronics" devices.

Among nonferromagnetic 3D metals, chromium occupies an important place[8] as it is frequently used in magnetic multilayers. Here, the knowledge of surface magnetic and electronic properties of the Cr surface plays a crucial role for the understanding and therefore proper construction of such multilayers. Already in the 1970s, it was theoretically recognized that the Cr(001) surface is ferromagnetic with a huge magnetic moment ($2.4\mu_B$-$3.0\mu_B$) in comparison to the bulk ($0.59\mu_B$).[9,10] However, the surface magnetic moment obtained experimentally varies significantly [$1.7\mu_B$ (Ref. 11)-$2.4\mu_B$ (Ref. 12)]. It has been pointed out in Ref. 12 that the significant scattering of experimental data on Cr is caused by surface defects and contamination which influence the reported data. Here, scanning tunneling spectroscopy (STS) can be of high value as it permits to obtain conclusive knowledge about electronic structure of perfect surfaces and of defects on an atomic scale. The STS experiments data for Cr(001) surface at room temperature show the existence of a strong surface resonance near the Fermi level.[11] The spin-polarized STS experiments[13] used this resonance to probe the magnetic structure of the Cr surface near monoatomic steps.

In this paper we present new experimental results obtained by low-temperature scanning tunneling microscopy and spectroscopy measurements as well as state of the art calculations of the electronic properties of the Cr(001) surface which allow us to understand to the full extent the novel experimental findings on this important surface. Brief information about part of the results has been published in Ref. 6.

## II. SAMPLE PREPARATION AND MEASUREMENT TECHNIQUE

For a detailed *in situ* analysis of sample surfaces, a low-temperature STM has been used with a sample cleaver at 4.2 K.[14,15] Since the vacuum pot with the STM inside is immersed into liquid helium, the vapor pressure of oxygen inside is extremely low ($<10^{-15}$ Torr); therefore, sample surfaces can stay clean for many days. The absence of thermal drift and high stability permitted images of $200\times200$ pixels and 200 $I/V$ points per pixel in spectroscopy mode to be obtained. In addition, high-resolution spectroscopy measurements were possible because at 4.2 K the thermal broadening in $dI/dV$ is only $3.5k_BT\approx1.4$ meV. All measurements were performed with mechanically cut PtIr tips.

 

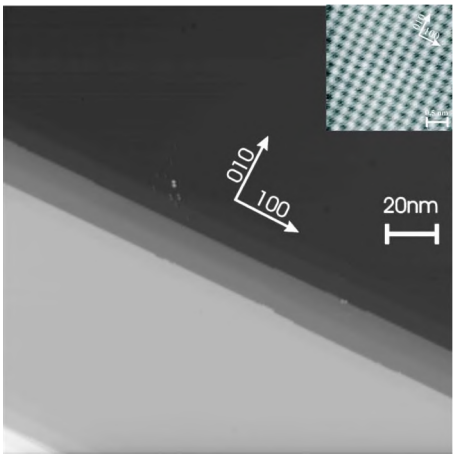


FIG. 1. (Color online) Topographic image (100 nm $\times$ 100 nm; $V_s$=−400 mV; $I$=100 pA) of cleaved Cr(001) surfaces. The crystallographic directions are shown by arrows. In the image a double tip effect can be seen. Inset: The atomically resolved Cr(001) image with a scan range of 3 nm $\times$ 3 nm. No image processing was performed apart from plane subtraction. The apparent corrugation is 1.5 pm at ($V_s$=−50 mV and $I$=0.5 nA). No residual surface contamination was found.

In order to obtain atomically clean Cr(001) surfaces for studies at liquid helium temperatures we have used a novel method of chromium single crystal cleavage which we have developed earlier.[16] For many years investigations of transition metals and particularly of Cr have been hampered due to severe experimental difficulties. Even after Cr sample cleaning by extended cycles of $Ar^+$ ion etching and annealing over a time period of several hundred hours, topography scans show the presence of impurities[17,18] caused by segregation of residual contaminations to the surface during the annealing procedure. This experimental bottleneck has not allowed STS measurements to be performed on atomically clean Cr surfaces of bulk single crystals and at low temperatures so far.

On the contrary, this technique allows us to produce the Cr(001) surfaces at liquid helium temperatures by cleavage of a Cr sample which was cut from a 99.99% chromium single crystal by spark erosion along the [001] direction. As we found[16] the cleaved surfaces consist of monatomic clean terraces with the widths from a few to several hundred nanometers belonging to the (001) cleavage plane. We also found that the Cr(001) cleavage plane yields [100] and [110] steps.

A typical STM image of the cleaved surface is shown in Fig. 1. It shows that the Cr(001) plane offers two independent directions for crack propagation at an angle of 45° to each other. From atomic resolution images these two directions can be identified as [100] and [110] crystallographic directions. The inset shows the image of the atomically resolved Cr(001) lattice with the fourfold symmetry of bcc (001) surfaces and an apparent corrugation of 1.5 pm. The atomically resolved STM images taken at different places on the cleaved surface showed that the concentration of impurities on the surface does not exceed the bulk concentration, e.g., the brittle fracture process does not appear to cause segregation of impurities to the surface.

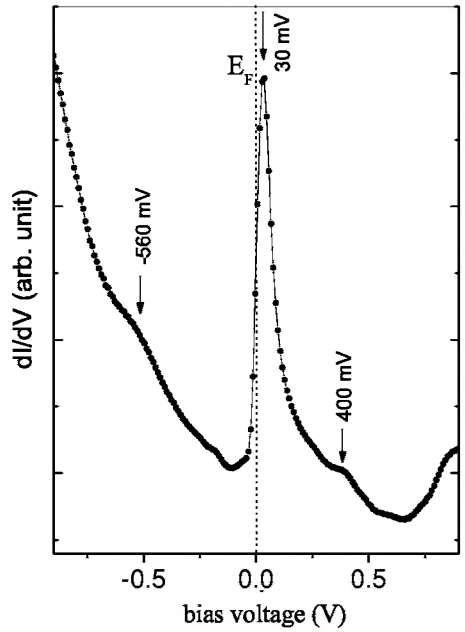


FIG. 2. Averaged tunneling conductance vs sample bias voltage ($dI/dV$) measured in the middle of a Cr(001) terrace of 50 nm wide. The $I_T$ vs $V_s$ curve was obtained using 200 points in the energy window of ±1 V. Numerical $dI/dV$ was obtained using 5 point differentiation. The setpoint during spectroscopy was $I$=1 nA, $V_s$ =−1 V.

## III. EXPERIMENTAL RESULTS

It is well known that the scanning tunneling spectroscopy technique can be employed to investigate surface electronic structure with atomical spatial resolution. Figure 2 shows the tunneling conductance spectrum ($dI/dV$) of the Cr(001) surface averaged over a 10 nm $\times$ 10 nm atomically clean surface area in the middle of a monatomic terrace of 50 nm wide. The spectrum can be characterized by a very strong and narrow feature located at around 30 mV above the Fermi level defined as $V_b$=0. In addition two shoulderlike features at around −0.5 V and 0.4 V can be seen. Measurements by STS $dI/dV$ characteristics are always convolutions of sample and tip electronic structures, therefore one has to be careful that features observed in tunneling spectra are derived from the sample and not from the tip. We have observed that the spectra measured above a particle which has been produced during the cleavage or has been dropped from the tip were featureless. Also the observed features have been very well reproduced (position and width) on different surfaces produced by fracture of four samples with four different tips. Although the intensity of the peak at 30 mV can vary due to different tips, the shape remains unchanged. Also it can be concluded that for peaks with higher intensity the peak become broader in such a way that the characteristic width remains constant. Therefore, we can conclude that the measured spectra reflect intrinsic properties of the Cr(001) surface and are not related to stress which might be introduced into the crystal during the fracture of the sample or tip properties.

As we mentioned above the Cr(001) surfaces produced by cleavage of a single crystal are atomically clean. However,

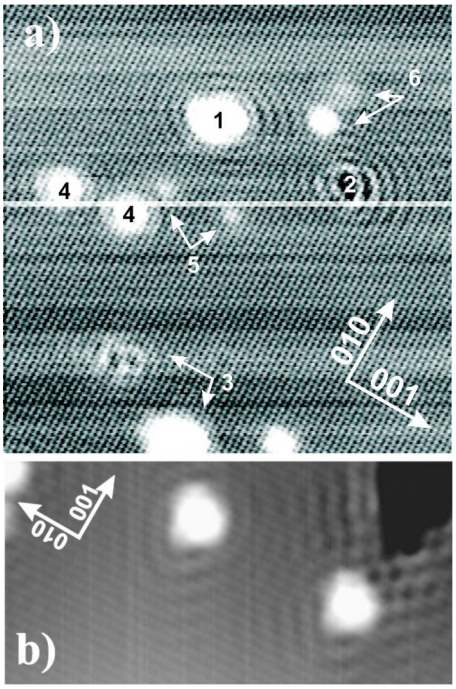


FIG. 3. (Color online) (a) 21 nm×21 nm and (b) 6.5 nm ×13.5 nm atomically resolved STM image taken at $V_b$=−50 mV and $I_T$=0.5 nA. Charge-density oscillations near single impurities and steps can be seen.

we found that it is possible to find surface areas where impurity concentration slightly exceeds the bulk concentration, probably, due to the existence of such "high" dopant zones in the crystal itself. Because the impurity concentration on such surfaces is still in the far submonolayer range, these "contaminated" surfaces can serve as a perfect playground for studying the influence of a single impurity on the electronic properties of the Cr(001) surface.

Figure 3(a) shows such a Cr(001) surface area with different types of impurities both in the first layer and buried in the subsequent layers. As one can see, the charge-density oscillations are set around different impurities (1, 2, 4, and 5). Around the impurities marked 5 and 6 no oscillations have been resolved due to the fact that they are probably located below the first layer and therefore the resulting oscillations will decay much faster than in the two-dimensional case.[19] It should be also mentioned that we observed these oscillations resulting from single steps which were present on the studied surface [see Fig. 3(b)].

From a line profile shown in Fig. 4 we can determine the period of the observed Friedel oscillations ($Q$ =0.97±0.05 Å$^{-1}$). It can be also determined from Fourier transformed (FT) STM images (see inset in Fig. 4), as has been proposed for the precise analysis of Friedel oscillations and for obtaining 2D Fermi contours of the studied surfaces in Refs. 20–22. It is worthwhile to mention the strong deviations of observed oscillations from the asymptotic behavior already at $r \leqslant 1.5$ nm which is of the order of five interatomic distances. This behavior is typical for the Kondo systems.[23,24]

Another characteristic of the observed Friedel oscillations on the Cr(001) surface is their anisotropy. As can be seen in

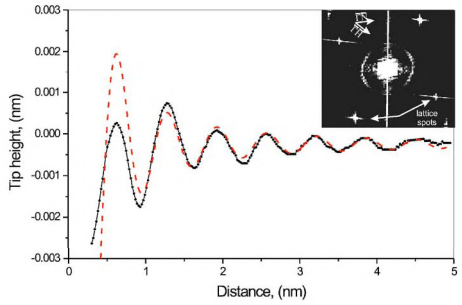


FIG. 4. (Color online) A line profile of the Friedel oscillations measured at $V_b$=50 mV. The dashed curve shows a fit by a $A\cos(Qr)/r^b$ function. The obtained fit parameters are $b$=1.5±0.2, $Q$=0.97±0.05 Å$^{-1}$. The inset shows 2D Fourier transform (power spectrum) of a STM image with Friedel oscillations. Four lattice spots can be seen and can be used for internal calibration. The fourfold symmetry of Friedel oscillations in ⟨011⟩ crystallographic directions can be seen as a four segment circle.

Fig. 3 the oscillations are not circular but have a distinctive asymmetry. They propagate in four crystallographic ⟨011⟩ directions and are suppressed in ⟨001⟩ directions. They are also kind of flattened in the ⟨011⟩ direction. The same anisotropy is also seen in FT images. In the inset in Fig. 4 the spots marked "lattice spots" are used for internal calibration of an FT image because they are the reciprocal lattice vector positions in the $\bar{\Gamma}\bar{H}$ direction. The four-segment circle centered at the origin is caused by Friedel oscillations around impurities. The anisotropy of these oscillations cause the reduction of the circle intensity in the $\bar{\Gamma}\bar{H}$ directions.

## IV. ONE-PARTICLE ELECTRONIC STRUCTURE AND FRIEDEL OSCILLATIONS

In order to clarify the experimental results we have performed first principle calculations of the electronic structure for the Cr(001) surface. The electronic structure of this surface has been addressed in a number of publications,[9–12,25–28] using different methods from simple tight-binding approximation, until the highly accurate FLAPW scheme. Unfortunately, there were no calculations of the surface nesting properties and magnetic susceptibilities. We therefore start with the density functional investigation of the Cr(001) surface and later analyzed many-body correlation effects.

All calculations have been done using the *ab initio* VASP method.[29,30] It is based on the local spin density functional theory and uses the PAW scheme.[31,32] Exchange and correlation potential[33] were described by the Perdew-Zunger[34] functional with nonlocal corrections to the exchange and correlation taken into account by a generalized gradient approximation (GGA) (Ref. 35) with the spin interpolation by Vosko *et al.*[36] The Cr(001) surface is modeled by an eight layer slab of relaxed Cr atom with a vacuum of 6.8 Å. The Brillouin zone integrations are performed on an 12×12×2 $k$-point grid with a first order Methfessel-Paxton smearing[37] using $\sigma$=0.2 eV. Starting from the bcc crystal structure with lattice parameter $a$=2.85 Å the slab was allowed to relax in the (001) direction until the forces on the atoms were smaller

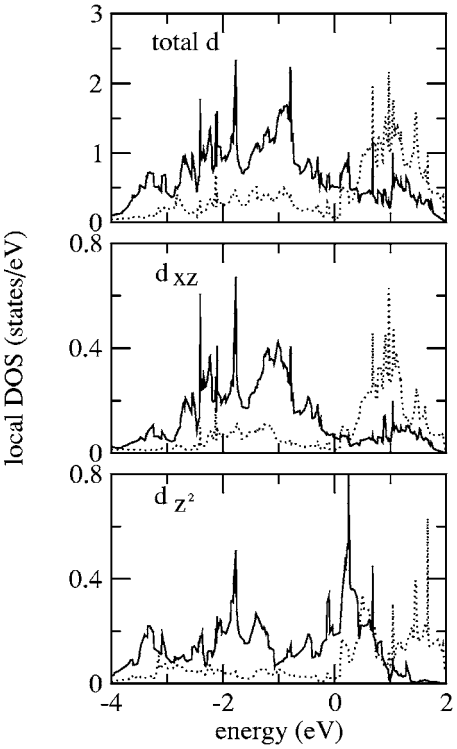


FIG. 5. The total density of states for Cr(001) surface layer together with the partial DOS ($d_{z^2}$ and $d_{xz}$) relative to the Fermi energy. The solid (dotted) curves correspond to the majority (minority) spin states.

than 0.02 eV/Å. From the calculations, the first interlayer distance was decreased by 5.5% and the second expanded by almost 4.5%. The magnetic moment of the surface atom increased to $\mu_S=2.4\mu_B$ and to $\mu_{S-1}=-1.3\mu_B$ in the subsurface layer in a good agreement with the previous computational results.[38,39]

Figure 5 shows the density of states of the surface layer. In general, the structure of calculated DOS is in agreement with previous band structure calculations.[25] There are two different surface states, corresponding to $d_{z^2}$ and $d_{xz}(d_{yz})$ orbitals. The most localized $d_{z^2}$ surface state is located approximately at 0.3–0.5 eV above the Fermi level for both spin-projections. The degenerate $d_{xz}$ and $d_{yz}$ surface states are more delocalized and located around −1 eV for spin-up states and close to 1 eV for negative spin-contribution (Fig. 5). If we compare the calculated DOS with experimentally measured $dI/dV$ spectra which are proportional to the electronic density of states on the surface we find out that the feature in the spectra at 0.4 eV above the Fermi level corresponds very likely to the surface state with mostly $d_{z^2}$ orbital character. This is also in agreement with previous calculations.[11,12] The feature at 0.5 eV below the Fermi level is not so strongly pronounced in the calculated DOS but still can be seen in Fig. 5 for the spin-up component of the $d_{z^2}$ electronic density of states at the Cr(001) surface. The most pronounced peak at around 30 meV above the Fermi level which has been measured experimentally cannot be seen in the calculated spectra at all. This drastic difference will be discussed in the next section of this paper. We would also like to draw attention to two spin-splitted $d_{xz}$, $d_{yz}$ surface states which can be seen in Fig. 5. These states were calculated for the first time by Klebanoff *et al.*[12] Experimentally these states can hardly be observed by the STS technique due to their position far from the Fermi level and strong hybridization with other states.

Another phenomenon which can be understood with the help of our calculations of the surface electronic structure of Cr(001) are Friedel oscillations around surface imperfections. Friedel oscillations are long-range modulations in the charge density which were predicted first by Friedel[40] nearly 40 years ago and are set by itinerant electron states which are scattered by the defects and interfere with themselves. Note that Friedel oscillations provide the primary mechanism for long-range interactions between adsorbed particles[41] and magnetic interactions between two nuclei.[42]

Although the Friedel oscillations result in the modulation of the total density of states (DOS), they can be also resolved by scanning tunneling microscopy (STM) as spatial modulations of local DOS around the Fermi level, as has been recently demonstrated on metal[20–22,43–45] and semiconductor[14] surfaces.

The Friedel oscillations are caused by the sharp discontinuity of the electron distribution function at the Fermi surface which leads to singularity of the screening function (static polarization operator) $\Pi(\mathbf{q},\omega=0)$ at the wave vector $\mathbf{q}$ equal to the diameter of the Fermi surface in the corresponding direction, $Q=2k_F$.[46] Long-range tail of charge density distribution around the defect $\rho(\mathbf{r})$ is determined by the Fourier transform of a singular contribution to $\Pi(\mathbf{q},0)$ at $x=|\mathbf{q}-\mathbf{Q}|\to 0$. These contributions are proportional to $x\ln x$, $\sqrt{x}$, and $\ln x$, for a generic cases of three-dimensional (3D) electron gas, two-dimensional (2D) electron gas, and for a peculiar "nesting" case (flat parts of the Fermi surface), correspondingly (for review, see, e.g., Ref. 47). The period of the oscillations are equal to $2\pi/Q$ and their amplitude for the case of point defects decays as $1/r^{1+\alpha}$ where $\alpha=2$ and 1 for a generic 3D and 2D cases, correspondingly, $\alpha=1$ and 1/2 for 3D and 2D cases under the "nesting" conditions. STM measures not the $\rho(\mathbf{r})$ but the spectral density at the Fermi energy, $\rho(\mathbf{r},E_F)$ which decays more slowly, like $1/r^{\alpha}$, since it is proportional to the derivative of $\rho(\mathbf{r})$ with respect to $k_F$. Therefore an information about cross sections of the Fermi surface, presence or absence of the "nesting" features, surface (2D) or bulk (3D) electron states is necessary for the description of corresponding STM data.

Thus, the observations of the Friedel oscillations on metallic surfaces gave a great opportunity to obtain unique information on 2D Fermi contours,[20–22] dispersion of free-electronlike surface states (even those which are not centered around $\bar{\Gamma}$ point),[43,44,48] and lifetimes of surface-state electrons.[19,49]

As we mentioned above mostly Friedel oscillations were observed on surfaces with surface electron states which have free-electronlike dispersion. However, for the case of Cr(001) surface, it is known, both experimentally and theoretically, that there are no free-electronlike surface states. Another interesting peculiarity which has to be considered for chromium is a charge density wave accompanying the

spin-density wave.[18] It was shown[18] that the bulk charge density wave in Cr gives rise to significant charge density modulations at the Cr surface. These type of oscillations have the following distinctive properties: (i) they are undisturbed by steps, adsorbates, or segregated surface contaminants; (ii) the overall wave pattern shows no dispersive behavior; (iii) they are largely suppressed at the Cr(001) surface. The above mentioned characteristics of these bulk charge density waves allow us to conclude that we are not dealing with the same effect but with truly surface Friedel oscillations.

For comparison with experiment, we calculated the Friedel wave function from our first principles calculations. As stated above, the Friedel wave vector corresponds to a singularity in the polarization, or equivalently in the electronic susceptibility. Therefore, one can easily identify the Friedel wave vector from a plot of the quantity

$$\zeta(\mathbf{q}) = \sum_{nn'\mathbf{k}} |\psi^{LR}_{n\mathbf{k}}|^2 |\psi^{LR}_{n'\mathbf{k}+\mathbf{q}}|^2 \delta(\epsilon_{n\mathbf{k}} - \epsilon_F)\delta(\epsilon_{n'\mathbf{k}+\mathbf{q}} - \epsilon_F) \propto \lim_{\omega\to 0} \frac{\mathrm{Im}\,\Pi(\mathbf{q},\omega)}{\omega},$$

where $|\psi^{LR}_{n\mathbf{k}}|^2$ is the local electron density at site $R$ for angular momentum $L=(l,m)$, band $n$, and crystal momentum $\mathbf{k}$. This function has the same singularity points as the static polarization operator $\Pi(\mathbf{q},0)$, but these singularities are much more pronounced and therefore it is widely used to investigate the nesting features of the Fermi surfaces.[50] It is important to stress that the contributions of partial $s$, $p$, and $d$ states to the amplitude of the Friedel oscillations are proportional to $\sin\delta_l$ (where $\delta_l$ are the corresponding phase shifts[46]). Therefore for the case of $s$-, $p$-defects such as C, O, N, and S atoms the contribution of the $d$-electrons is negligible. Figure 6 shows the Fermi surface projected to the Cr(001) together with the contribution of the $s$- and $p$-electrons to the $\zeta(\mathbf{q})$ function. One can clearly see the broad ridge of susceptibility maximum at approximately experimental values of the **Q**-vector. The Friedel wave vector can now be estimated to be 0.97 Å$^{-1}$.

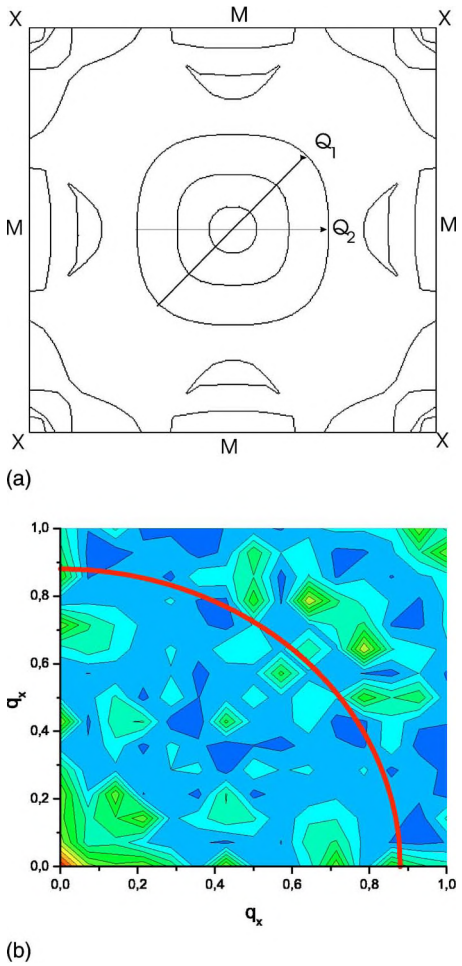


FIG. 6. (a) (Color online) Projection of the Fermi surface for Cr(001); the main nesting vectors are labelled by $Q_1$ and $Q_2$. (b) The contribution of $s$-, $p$-electrons to the "nesting function" $\zeta(\mathbf{q})$ shown by the intensity of gray scale together with the average position of experimentally observed maximum of Fridel oscillations at ($Q$=0.97 Å$^{-1}$) (the bold circle).

## V. MANY-ELECTRON EFFECTS

In this section we will discuss in full details the experimentally observed peak in the Cr(001) density of states which is located at about 30 meV above the Fermi level (see Fig. 2). As we have shown recently[6] this feature in the density of states cannot be described in the framework of one-electron picture but many-electron effects have to be taken into account. These many-body calculations showed that this peculiar state in the Cr(001) electronic structure can be considered as a manifestation of an orbital Kondo resonance.

The Kondo effect is a fascinating, essentially many-body quantum phenomenon. It was discovered experimentally about 70 years ago[51] as an anomalous resistivity minimum for diluted magnetic alloys at low temperatures. The explanation of this phenomenon came only in the 1960s[52] and became the starting point of the progressively developing field of many-electron physics. The Kondo effect is connected with the interaction of localized spin moment with itinerant electrons of a host metal (spin-flip scattering). This scattering leads to a highly correlated many-body ground state where the conduction electrons form a spin polarized cloud around the magnetic impurity. The low-energy excitations of this screening cloud lead to the formation of a narrow resonance at the Fermi level, Abrikosov-Suhl, or Kondo, resonance.[53,54] Two important parameters for the Kondo problem are temperature and magnetic field. If the temperature becomes higher than some characteristic temperature ($T_K$), the correlations between the impurity spin and the conduction electrons are broken and the Kondo effect disappears. The magnetic field also influences the Kondo effect due to the fact that the degeneracy of the two states between which the spin-flip occurs (spin up and spin down quantum states) is very important. In this way the applied magnetic field destroys the degeneracy leading to disappearance and/or splitting of the Kondo resonance.

During the last 40 years the "Kondo physics" has been extensively explored and evolved into one of the most interesting and general many-particle phenomena. Apart from di-

luted magnetic alloys it is also extensively explored in the broad spectrum of problems connected with heavy fermion physics.[54] Recently with the development of nanotechnology it appears that also here the Kondo effect is very important. It has been found in nanoscale electronic devices[55,56] and carbon nanotubes.[57,58]

Scanning tunneling microscopy, which is well known as an excellent tool to investigate the atomic structure of conductive surfaces, can be also employed to explore many-body phenomena, such as the formation of the Kondo resonance[57,59–63] or $d$-wave pairing in copper-oxide high-$T_c$ superconductors.[64] The unique STM ability to observe the Kondo effect in real space brings a new excitement into a "classical" Kondo problem, as has been shown recently by forming a quantum mirage of a magnetic atom.[60] In an experiment on a single magnetic atom[59–63] the Kondo resonance was observed as an asymmetric dip in $dI/dV$ spectra due to the Fano effect.[65] This effect is related to the fact that the conduction electrons dominate in the STM-current, but their spectral density is redistributed through the scattering with the localized electrons. Theory of the Fano effects in the STM spectra was developed in Refs. 66 and 67. It has been also found[59] that the contribution from the localized electron states decreases as the tip moves away from the atom's center, whereas the contribution of itinerant electron states remains constant. However, in an experiment on Co clusters deposited on single-walled carbon nanotubes,[57] the Kondo resonance was seen as a peak in $dI/dV$ spectra indicating that the tunneling into localized states dominates over the continuum channel. The authors speculated that this difference is connected with the detailed characteristic of the nonmagnetic host but the exact answer remains unknown.

After the discovery of the Kondo effect in diluted magnetic alloys, it has been realized that the main idea, namely, flip scattering processes between conduction electrons and internal degrees of freedom (spin in the case of a magnetic atom), can be generalized for scattering centers with nonspin degrees of freedom. In principle, nothing rules out such a Kondo effect out provided that there are two truly degenerated states on the tunneling center or impurity ion. Since the mid-80s, there has been a large body of experiments arising from tunneling centers in metals, actinide ions in metals, electric dipoles in metals and more recently quantum dots in the Coulomb blockade regime.[68–70] Pseudospin Kondo effect for strongly anharmonic crystals were considered also in the context of the theory of high-temperature superconductivity.[71]

The tight-binding mean-field calculations for the ferromagnetic Cr(001) surface,[12] as well as our results presented in the previous section, demonstrate the existence of two degenerate spin-split $d_{xz}$, $d_{yz}$ surface states located about 1 eV below and above the Fermi level. The spatial symmetry of these states on (001) surface protects the degeneracy and the interaction of such states with the conduction electrons can lead to the formation of a many-body Kondo resonance near the Fermi level. The $d_{xz}$ state, being hybridized with the conduction electron bands, changes into the $d_{yz}$ state via virtual many-body excitations, and vice versa. In this process a many-body "orbital singlet" can be formed, with the $d_{xz}$, $d_{yz}$ states mixed symmetrically in the surface plane, similar to the spin-flip mechanism of the local magnetic moment screening in the conventional Kondo effect.[69] These orbital flips lead to the formation of a many-electron resonance at the Fermi energy—the orbital Kondo resonance. Since we have the whole lattice of the resonant scattering centers (every surface atom), a narrow quasiparticle band is formed near $E_F$, similar to the formation of the heavy-fermion state in the spin Kondo lattices.[54] It is important to stress that we consider the orbital Kondo resonance due to a double degeneracy of the $d_{xz}$, $d_{yz}$ states and not the spin one since the spin degeneracy is broken by the ferromagnetism of the Cr(100) surface.[13]

In order to verify the formation of the orbital Kondo resonance on the Cr(001) surface quantitatively, we have carried out calculations for the periodic degenerate Anderson model[54,72] with the Hamiltonian

$$H = \sum_{km\sigma} [E_0^{\sigma} f_{km\sigma}^{+} f_{km\sigma} + \varepsilon_{km\sigma} c_{km\sigma}^{+} c_{km\sigma} + V^{\sigma}(c_{km\sigma}^{+} f_{km\sigma} + f_{km\sigma}^{+} c_{km\sigma})] + \frac{1}{2} \sum_{i,m,m',\sigma,\sigma'} U_{m,m'}^{\sigma\sigma'} n_{im\sigma} n_{i,m',\sigma'}, \quad (1)$$

where $f_{km\sigma}$, $c_{km\sigma}$ are the annihilation operators for localized and itinerant states, correspondingly, $k$ is the wave vector, $\sigma$ is the spin projection, $m=1,2$ corresponds to $d_{xz}$ and $d_{yz}$ surface states for the localized electrons, and $sp$ band indices for itinerant electrons with the spectrum $E_0^{\sigma}=E_0-\sigma H$ is the on-site $d$-energy, $H$ is the spin splitting, $V_{\sigma}$ is the effective spin-dependent hybridization parameter, $U_{m,m'}^{\sigma,\sigma'}$ is a rotationally invariant Coulomb matrix for the two-orbital model defined via the effective Hubbard repulsion $U$ and Hund exchange $J$ energy, correspondingly, $n_{im\sigma}=f_{im\sigma}^{+} f_{im\sigma}$ and $i$ is the site index. For qualitative description of the experimental results, we used a simple semicircular model for conducting $sp$-bands with a total bandwidth of 4 eV and effective hybridization parameters of 0.4 and 0.5 eV for spin-up and spin-down interactions, respectively, which simulate the ferromagnetic surface of chromium.[12] In fact the position of spin-split maximum in the $d_{xz}$ and $d_{yz}$ are reproduced in our eight-atoms slab calculations. In our model many-body calculations for the Cr(001) surface we chose the value of the Coulomb interaction parameter $U=1.2$ eV describing the metallic screening of electron-electron interactions on the $d$-electrons surface and the effective exchange interaction $J=0.4$ eV. The last assumption is qualitatively correct provided that their bandwidth is smaller than $U$, so they are on the insulating side of the Mott transition in the corresponding band. Otherwise they will form a band with **k**-dependent energy spectrum, and an exact symmetry in $xy$ plane will take place only for $\Gamma$ point. Of course, it does not mean that the Kondo effect is impossible in the latter case (cf. with the discussion of the Kondo effect in ferromagnetic Kondo lattices[73] or Kondo resonance in the Hubbard model near the Mott transition[72]), but its consideration should be more complicated. Here we restrict ourselves to the simplest model which allows us to explain the experimental results qualitatively. The average position of the $d_{xz}$ and $d_{yz}$ surface states, effective bandwidth as well as their exchange splitting are in

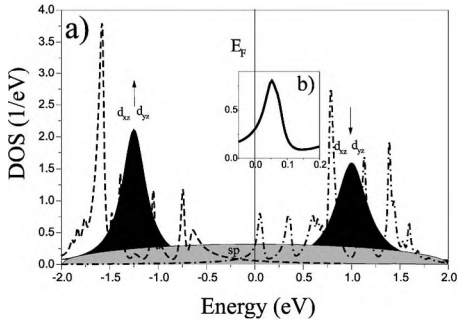


FIG. 7. (a) Spin-polarized density of states (DOS) for the two-degenerate periodic Anderson model (parameters see in the text). The bare DOS consisting of conduction electrons and $d_{xz}$, $d_{yz}$ surface states is shown by filled area. The corresponding DOS for correlated electrons is shown by dashed and dashed-dotted curves for majority and minority states respectively. (b) Orbital Kondo resonance on a larger scale.

qualitative agreement with our surface band structure calculations (Fig. 5).

In order to solve the problem, we use the dynamical mean-field theory (DMFT, for review see Ref. 72), which is considered as a reliable approximation in lattice many-body models and was used for the investigation of the electronic structure for a one-band periodic Anderson model in Ref. 74. The effective impurity problem has been solved by the exact diagonalization technique[72] with the six effective states in the electronic bath function. The results of the calculations are shown in Fig. 7(a). The orbital Kondo resonance, in the vicinity of the Fermi level [Fig. 7(b)], forms under very general conditions. A reasonably small intrinsic bandwidth for $d_{xz}$, $d_{yz}$ states cannot destroy it since the Kondo resonance is also known for the itinerant-electron Hubbard model.[72] The characteristics of spectra for larger energies ($|E-E_F|>0.3$ eV) are more sensitive to the details of the real conduction band structure.

It is clear that the exact diagonalization scheme can prove the existence of the Kondo resonance in multiorbital case, but is insufficient to reproduce its exact shape and position due to limitations of available Hilbert space. One can show from general qualitative arguments, based on the Friedel sum rule that for the multichannel assymetric Anderson model, the Kondo resonance may be shifted from the Fermi level.[54] In order to verify this result quantitatively we have done the numerical renormalization group (NRG) (Ref. 75) calculations for the two-band impurity Anderson model.[76] The computational results (Fig. 8) show the narrow Kondo resonance above the Fermi level. These NRG results support the idea that the Kondo resonance is really shifted from the Fermi level in the multiband case, which is one of the main features of the experimental STM spectra as well as the DMFT calculations.

Let us now discuss the experimental results obtained by STM and STS on the Cr(001) surface in the framework of the orbital Kondo effect described above. As we mentioned above a Kondo resonance is always located near the Fermi level due to its many electron nature, therefore a many-particle model is consistent with the experimental observation of a peak in the Cr(001) surface density of states so close to the Fermi level (26 meV) which is shown in Fig. 3. The experimentally observed width of the peak also points to the many-electron nature of the resonance. The width of a Kondo resonance is determined by the Kondo temperature[54] and therefore can be very small. The asymmetrical line shape of the peak suggests that a Fano model[65] has to be used in order to analyze it quantitatively. This model was considered to be a reliable approximation for analysis of Kondo resonances observed by STS.[59] The interference between noninteracting discrete channels and a continuum may be expressed in terms of the rate of transition to a final state of energy $\varepsilon$

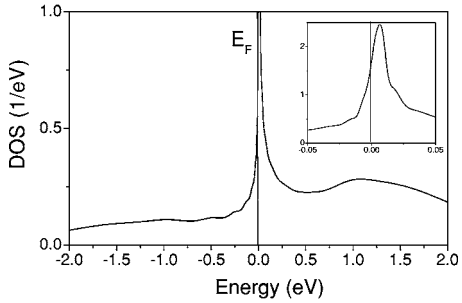


FIG. 8. The density of states for the two-degenerate impurity Anderson model with the rectangular bare DOS of the half bandwidth 2 eV($U=2$ eV, $J=0.2$ eV, $E_0=-1$ eV, $V=0.35$ eV). In the insert the Kondo resonance on a larger scale is shown.

$$R(\varepsilon) \propto R_0(\varepsilon)\frac{(q+\varepsilon')^2}{1+\varepsilon'^2}, \quad \varepsilon' = \frac{\varepsilon-\varepsilon_0}{\Gamma/2}, \tag{2}$$

where $\varepsilon_0$ is the energy of the discrete state, $\Gamma$ is the width of the resonance, $R_0(\varepsilon)$ is the transition rate as it would be in the absence of the discrete state, and $q$ is the ratio of the matrix elements linking the initial state to the discrete and continuum parts of the final state. As has been shown in Ref. 59, the parameter $\Gamma$ gives directly the Kondo temperature of the corresponding resonance ($\Gamma=2k_BT_K$). A fit by the Fano shape to the experimental spectrum is shown in Fig. 9 by the solid curve. As can be seen the Fano model describes the experimental line shape very well including a dip at the Fermi level. There is an essential difference between our

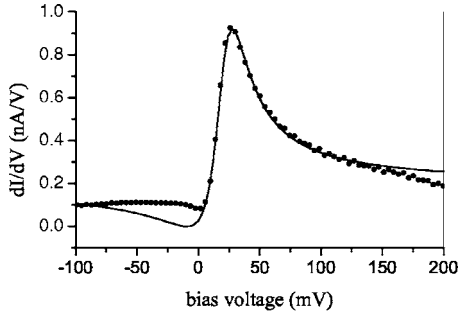


FIG. 9. Averaged tunneling conductance vs sample bias voltage measured in the middle of a Cr(001) terrace of 70 nm width is shown by dots. The solid curve shows a fit by the Fano shape with $T_K=15$ meV, $q=1.9$, and $\varepsilon_0=20$ meV.

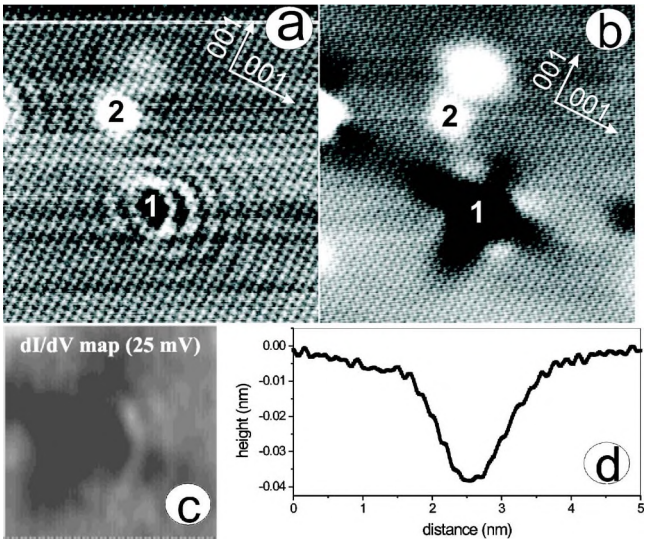


FIG. 10. (Color online) (a), (b) 10 nm×10 nm STM images obtained at $I$=0.5 nA and $V_b$ equal to (a) –50 mV, (b) 25 mV. (c) A $dI/dV$ map plotted at bias voltage of 25 mV corresponding to the resonance energy. A dark crosslike feature corresponds to the suppression of the peak amplitude mapped in the real space. (d) A line profile taken along the depression which is shown in (b).

STS data, concerning the orbital Kondo lattice, and the previous experimental results on the spectroscopy of Kondo resonances for isolated magnetic impurities.[59–63] In the latter case the resonance in the density of states is observed experimentally as a Fano-type dip in $dI/dV$. The corresponding parameter $q$ in the Fano model was about 0.7 indicating that the continuum channel mostly contributed to the tunneling in those cases. In our case we found that the $q$ parameter describing the line shape of the peak is 1.9 indicating that in the case of the orbital Kondo lattice $d_{xz}$, $d_{yz}$ surface states contribute directly to the current, which results in the resonance in the $dI/dV$ spectra. A similar effect is well known in heavy-fermion physics where heavy $f$-electrons contribute to the superconductivity, de Haas-van Alphen effect, etc.[54] In our case, the tunnel current of $d_{xz}$, $d_{yz}$ states can overshadow the contribution of itinerant electrons. We would like to point out that the shape and the width of the Cr(001) resonance is strikingly similar to the Kondo resonance observed on Co clusters where $T_K$=16 meV and $q$=3.3 were found. In the context of discussion of the STM spectra for isolated Kondo impurity versus the Kondo lattice it is worthwhile to mention that the Kondo resonance cannot be observed in the tunneling spectra for the case of homogeneously distributed impurities.[3] However, for the case of magnetic impurity monolayer the Kondo effect should be observable as was experimentally confirmed in Ref. 77. In our case the spin-polarized surface chromium layer plays a very similar role.

Figure 10(a) shows a STM image of the Cr(001) surface with different types of impurities. The charge density oscillations set around the impurities in order to screen the local potential can be seen. This oscillation pattern persists for all energies but for the narrow region (5 meV$<V_b<$40 meV) corresponding to the Kondo resonance it is suppressed in the vicinity of the impurity. A STM image obtained at the bias voltage corresponding to the resonance energy (Fig. 10(b)) shows crosslike depressions centered around impurities. The size of this feature is about 4.5 nm in the ⟨100⟩ directions. Coexistence of the crosslike feature and the Friedel oscillations is clearly seen in Fig. 10(c).

We found mostly two types of impurities on the cleaved surface: one is seen as protrusions [e.g., 2 in Figs. 10(a) and 10(b)] corresponding probably to S, and another is seen as depressions [e.g., 1 in Fig. 10(a)] corresponding probably to N, O or C, as these elements are most common for a Cr single crystal.[17] Although the exact origin of point defects on the Cr(001) surface is unknown, it is important to notice that the crosslike feature appears on both types of impurities and is related to the intrinsic electronic property of the Cr(001) surface. This depression is the result of a decrease of the density of states at the energy corresponding to the resonance with crosslike spatial distribution, as can be seen from a $dI/dV$ map shown in the inset in the top of Fig. 10(c). A three-dimensional structure of this suppression can be seen in Fig. 10(d). The depth of this feature in the center is 40 pm and the depth of the wings extended in the [100] directions is about 10 pm. Also atomic corrugation inside the depression can be seen from line profiles in Fig. 10(c).

Let us discuss the possible origin of these "crosslike" features. It has been recently demonstrated that the symmetry of the order parameter in superconducting cuprates can be revealed by monitoring its destruction on defects.[64] As has been discussed in Ref. 78, this idea can be generalized: an impurity locally destroys a coherent state and allows to visualize the character and spatial symmetry of this state with the atomic scale STM probe. A Kondo resonance is a specific coherent many-body state with the order parameter an average of a "slave boson" operator.[54] Therefore the observed fourfold symmetry of depressions on impurities [Fig. 10(b)] directly reflect the wave character of the resonance.

As we have discussed above, we demonstrate that the orbital Kondo resonance on Cr(001) is formed by $d_{xz}$, $d_{yz}$ surface states which are mixed symmetrically in the surface plane. The corresponding fourfold symmetry of a resulting state corresponds nicely with the experimentally observed crosslike feature. Also the large extension of these depressions on impurities follows the proposed many-body model. In contrast to a one-electron state, for the Kondo resonance of many-electron origin, the narrow distribution in $k$-space leads to a large extension in real space with a characteristic radius $r_K \approx \hbar v_F / T_K$ where $v_F$ is the average Fermi velocity.[54] This estimation is based on the fact that the Kondo resonance, as well as Cooper pairs, are formed from a very narrow region in $k$-space near the Fermi surface. However, it should be pointed out that the $r_K$ only characterizes the origin of the effect but do not reflect the size of the "Kondo cloud" quantitatively. It has been also found that the spatial extension of a Kondo resonance from a magnetic atom observed by the STS technique[59–63] is much smaller than the theoretically predicted size of the Kondo cloud. Note also that the difficulties with the observation of the Kondo cloud for a "standard" Kondo effect are connected with the charge-spin separation; the charge response function turns out to be not sensitive to the Kondo effect.[79] In the case of *orbital* Kondo resonance the Kondo cloud effect should be better

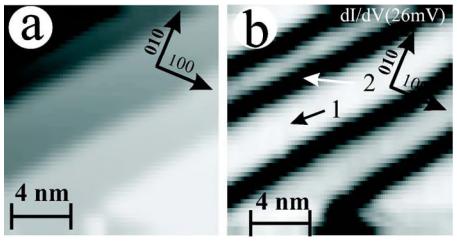


FIG. 11. (Color online) (a) Topographic image of the Cr(001) surface at a setpoint of $I=0.2$ nA and $V_s=-0.2$ V. The image shows a frame of 16 nm$\times$16 nm. The [110] terraces with a step height of 0.144 nm can be observed. (b) STM images of the surface area shown in (a). The image contains $100\times100$ pixels. Each pixel shows an amplitude of the tunneling conductance spectrum at $V_s=26$ mV (e.g., peak amplitude).

pronounced because of the higher sensitivity of tunnel current to orbital degrees of freedom than to the spin ones.

Also a step edge is a naturally formed one dimensional defect which destroys the symmetry of the Cr(001) surface. Figure 11(b) shows a spectroscopic image $(dI/dV)_{V_s}$ at the bias voltage corresponding to the peak position. One can see that step edges in both [110] and [100] directions can also be clearly seen in the spectroscopic image as dark lines (i.e., lower $dI/dV$ amplitude). From single curves shown in Fig. 12 for the terraces oriented in the [110] crystallographic direction one can see that under the approach to the terrace edge the peak amplitude decreases, the peak becomes broader, and shifts to higher energies. We also found that the observed shift of the peak energy in the close proximity to a terrace edge is more strong on narrow terraces. Figure 13 shows a dependence of the peak on the width of terraces oriented in the [100] direction. As can be seen similar to the spectra presented in Fig. 12, for narrow terraces the peak becomes broader and shifts to the higher energies, but the absolute value of the shift for a given characteristic distance from the step edge is approximately one order of magnitude larger for narrow terraces as compared to an isolated step edge.

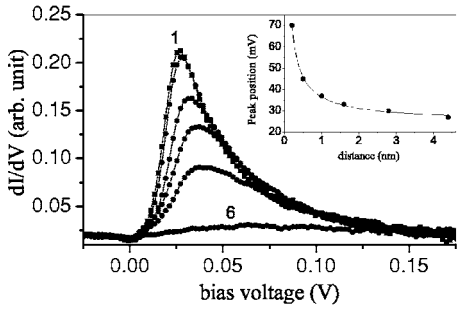


FIG. 12. Tunneling conductance vs sample voltage dependencies from the $dI/dV$ map shown in Fig. 11(b). $dI/dV$ were numerically differentiated from $I_T(V_s)$ measurements taken every 2 mV. Curves 1–6 were taken at distances 2.2±0.05 nm, 1.4±0.05 nm, 0.8±0.05 nm, 0.5±0.05 nm, 0.25±0.05 nm, and 0.1±0.05 nm, from the step edge, respectively. The inset shows the dependence of the peak position on the distance from the step edge oriented in the [110] crystallographic direction. The drawn lines are to guide the eye.

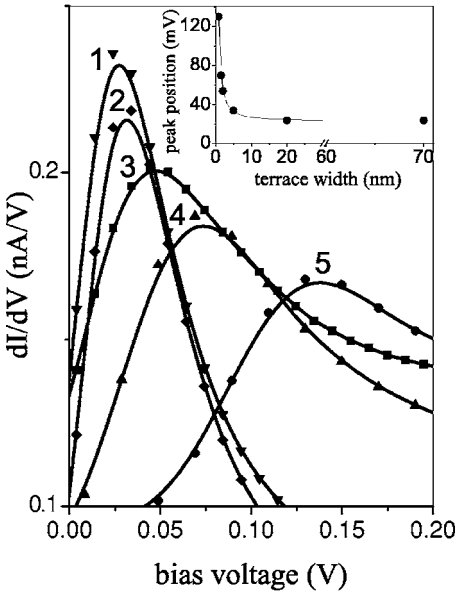


FIG. 13. Differential conductance spectra measured in the center parts of terraces with different widths. 1–5: peak positions are 24, 34, 54, 70, 130 mV measured on a surface area with average terrace widths of 20, 5, 2, 1.5, 0.8 nm, respectively. The drawn lines are to guide the eye. An inset shows the dependence of the surface state energy on the terrace width.

In a model of conventional (spin) Kondo a magnetic field has a pronounced influence on a Kondo resonance. It is even often called a hallmark of the Kondo effect that the magnetic field causes the splitting and broadening of the Kondo resonance at fields comparable to the Kondo temperature. However we have to point out that this picture is only valid for symmetric Kondo resonance (e.g., located on the Fermi level).[54] To the best of our knowledge there is no theoretical model treating the influence of a magnetic field on an asymmetrical Kondo resonance, although it has been observed experimentally,[57,60] but the influence of magnetic field was not reported. In the case of a Kondo resonance which is located not on the Fermi level the splitting of the Kondo peak under magnetic field or other perturbation would lead to the increase of the density of states on the Fermi level which is forbidden. Therefore, for the general nonsymmetric Kondo lattice problem the shifting and broadening of the many body resonance is a more general way of destroying the Kondo coherence.

The breaking of symmetry leads to the destruction of the $d_{xz}$, $d_{yz}$ surface state degeneracy and as a consequence the disappearance of the Kondo resonance. Following the analogy with the spin Kondo effect we can also introduce an effective "pseudomagnetic field" ($h_{\mathrm{eff}}^{\mathrm{orb}}$). The dependence of $h_{\mathrm{eff}}^{\mathrm{orb}}$ on the distance from the step edge (d) can be estimated in first-order perturbation theory to within the change of the total electron density. Similar to Friedel oscillations considered above, this leads to $h_{\mathrm{eff}}^{\mathrm{orb}} \propto d^{-3/2}$ for a general shape of the Fermi surface[45] and $h_{\mathrm{eff}}^{\mathrm{orb}} \propto d^{-1}$ for the case of a pronounced "nesting" on the Fermi surface. As can be seen in Fig. 14, the dependence of the peak energy as a function of the distance from the step edge follows the $d^{-1\pm0.2}$ law in agreement with the theoretical picture for the "nesting" of the Cr(001) Fermi

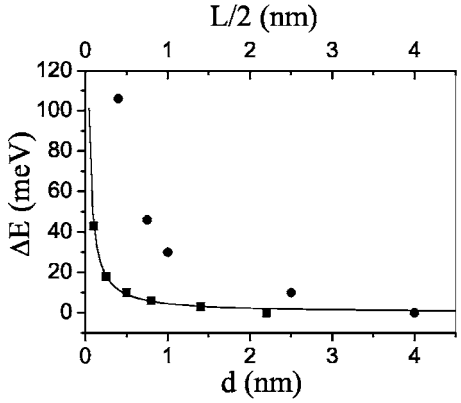


FIG. 14. The dots show dependence of the peak position on the terrace width plotted as a function of a half terrace width and the squares correspond to the peak position as a function of the distance from [110] step edges. The solid line presents the best fit which gives $\propto 1/d^{-1.1\pm0.2}$ dependency of the peak position as a function of the distance from the step edge.

surface which we also found experimentally from the Friedel oscillations. This effect of the shift of the peak position on monoatomic terraces is expected to double due to contributions from both step edges. However, as can be seen in Fig. 14 the peak shift observed on terraces is larger and continue to increase for narrow terraces becoming almost one order of magnitude larger on very narrow terraces. This fact can be understood by the interaction of perturbation centers (terrace edges) at sufficiently small distances. In this case the simple first-order perturbation theory approximation cannot describe the real picture any more and a more sophisticated theory has to be put forward.

## VI. CONCLUSIONS

The results of the low-temperature STM investigations of the Cr(001) surface presented here demonstrate how complicated the surface electronic structure may be even for elemental solids with simple crystal lattices. Whereas the density functional calculations seem to be adequate to explain the surface Friedel oscillations the essentially many-body physics manifests itself via the formation of a narrow density of states peak near the Fermi energy. Here we propose an interpretation of this peak in terms of the "orbital Kondo resonance" due to exact double degeneracy of different orbitals at the perfect surface; the defects such as the terrace edges break this degeneracy and, hence, destroy the resonance. Of course, further investigations, both experimental and theoretical, are necessary to understand the detailed bahavior of the resonance; from theoretical point of view we deal with a very complicated problem of the Kondo *lattice* with both spin and orbital degrees of freedom and complicated external fields created by the defects. It would be very important, also, to study another metallic surfaces to understand how general is this phenomenon. To form the resonance the system should have surface states with rather strong localization ($d_{xz}$, $d_{yz}$ in our case); however, an important difference between the one-particle picture and the many-particle one is that in the latter case these states can be initially not very close to the Fermi surface to produce the resonance so the necesssary conditions for its appearance do not look too restrictive. Also, it would be very interesting to investigate the difference between the Cr(001) surface where the spin degrees of freedom are strongly suppressed by the ferromagnetism and other bcc transition metals where both spin and orbital degrees of freedom may be essential.

After this work has been completed, we have learned about the recent temperature dependent STM-measurements on Cr(001) surface.[80] Different methods of the surface preparation (argon-ion etching and annealing) was used, but the low-temperature STM-spectra agreed very well with our data. The temperature dependence of the low-energy resonance is consistent with the Kondo-type behavior.

## ACKNOWLEDGMENTS

We are grateful to R. Wiesendanger, M. Bode, and K. von Bergmann for helpful discussions and for the information about Ref. 80 prior the publication. This work was supported to by the Stichting voor Fundamenteel Onderzoek der Materie (FOM) and by the Nederlandse Organisatie voor Wetenschappelijk Onderzoek (NWO Project No. 047.016.005).

[1] I. Giaever, Phys. Rev. Lett. **5**, 147 (1960).
[2] J. Bardeen, Phys. Rev. Lett. **6**, 57 (1961).
[3] J. Sólyom and A. Zawadowski, Phys. Kondens. Mater. **7**, 325 (1968); **7**, 342 (1968).
[4] A. Zawadowski, Phys. Rev. **163**, 341 (1967).
[5] J. A. Appelbaum and W. F. Brinkman, Phys. Rev. B **2**, 907 (1970).
[6] O. Yu. Kolesnychenko, R. de Kort, M. I. Katsnelson, A. I. Lichtenstein, and H. van Kempen, Nature (London) **415**, 507 (2002).
[7] P. LeClair, J. T. Kohlhepp, H. J. M. Swagten, and W. J. M. de Jonge, Phys. Rev. Lett. **86**, 1066 (2001).
[8] H. Zabel, J. Phys.: Condens. Matter **11**, 9303 (1999).
[9] G. Allan, Surf. Sci. **74**, 79 (1978).
[10] D. R. Grempel, Phys. Rev. B **24**, 3928 (1981).
[11] J. A. Stroscio, D. T. Pierce, A. Davies, R. J. Celotta, and M. Weinert, Phys. Rev. Lett. **75**, 2960 (1995).
[12] L. E. Klebanoff, R. H. Victora, L. M. Falicov, and D. A. Shirley, Phys. Rev. B **32**, 1997 (1985).
[13] M. Kleiber, M. Bode, R. Ravlić, and R. Wiesendanger, Phys. Rev. Lett. **85**, 4606 (2000).
[14] M. C. M. M. van der Wielen, A. J. A. van Roij, and H. van Kempen, Phys. Rev. Lett. **76**, 1075 (1996); M. C. M. M. van der Wielen, Ph.D. thesis, University of Nijmegen, 1998; E. J. G. Boon, Ph.D. thesis, University of Nijmegen, 1997.
[15] J. W. G. Wildöer, C. J. P. M. Harmans, and H. van Kempen, Phys. Rev. B **55**, R16013 (1997).

[16] O. Yu. Kolesnychenko, R. de Kort, and H. van Kempen, Surf. Sci. **490**, L573 (2001).
[17] M. Schmid, M. Pinczolits, W. Hebenstreit, and P. Varga, Surf. Sci. **377**, 1023 (1997).
[18] K.-F. Braun, S. Fölsch, G. Meyer, and K.-H. Rieder, Phys. Rev. Lett. **85**, 3500 (2000).
[19] Ph. Avouris, I. W. Lyo, and R. E. Walkup, J. Vac. Sci. Technol. B **12**, 1447 (1994).
[20] P. T. Sprunger, L. Petersen, E. W. Plummer, E. Lægsgaard, and F. Besenbacher, Science **275**, 1764 (1997).
[21] Ph. Hofmann, B. G. Briner, M. Doering, H.-P. Rust, E. W. Plummer, and A. M. Bradshaw, Phys. Rev. Lett. **79**, 265 (1997).
[22] L. Petersen, P. Laitenberger, E. Lægsgaard, and F. Besenbacher, Phys. Rev. B **58**, 7361 (1998).
[23] P. E. Bloomfield, R. Hecht, P. R. Sievert, Phys. Rev. B **2**, 3714 (1970).
[24] F. Mezei and G. Grüner, Phys. Rev. Lett. **29**, 1465 (1972).
[25] C. L. Fu and A. J. Freeman, Phys. Rev. B **33**, 1755 (1986).
[26] S. Blügel, D. Pescia, and P. H. Dederichs, Phys. Rev. B **39**, R1392 (1989).
[27] A. A. Ostroukhov, V. M. Floka, and V. T. Cherepin, Surf. Sci. **331–333**, 1388 (1995).
[28] G. Bihlmayer, T. Asada, and S. Blügel, Phys. Rev. B **62**, R11937 (2000).
[29] G. Kresse and J. Furthmüller, Phys. Rev. B **54**, 11169 (1996); Comput. Mater. Sci. **6**, 15 (1996).
[30] G. Kresse and J. Hafner, Phys. Rev. B **47**, R558 (1993); **49**, 14251 (1994).
[31] P. E. Blöchl, Phys. Rev. B **50**, 17953 (1994).
[32] G. Kresse and D. Joubert, Phys. Rev. B **59**, 1758 (1998).
[33] The modeled core used is Ne $3s^2$.
[34] J. P. Perdew and A. Zunger, Phys. Rev. B **23**, 5048 (1981).
[35] J. P. Perdew, J. A. Chevary, S. H. Vosko, K. A. Jackson, M. R. Pederson, D. J. Singh, and C. Frolhais, Phys. Rev. B **46**, 6671 (1992).
[36] S. H. Vosko, L. Wilk, and M. Nusair, Can. J. Phys. **58**, 1200 (1980).
[37] M. Methfessel and A. T. Paxton, Phys. Rev. B **40**, 3616 (1989).
[38] A. Eichler and J. Hafner, Phys. Rev. B **62**, 5163 (2000).
[39] G. Bihlmayer, T. Asada, and S. Blügel, Phys. Rev. B **62**, R11937 (2000).
[40] J. Friedel, Nuovo Cimento, Suppl. **7**, 287 (1958).
[41] K. H. Lau and W. Kohn, Surf. Sci. **75**, 69 (1978).
[42] M. A. Ruderman and C. Kittel, Phys. Rev. **96**, 99 (1954).
[43] M. F. Crommie, C. P. Lutz, and D. M. Eigler, Nature (London) **363**, 524 (1993).
[44] Y. Hasegawa and Ph. Avouris, Phys. Rev. Lett. **71**, 1071 (1993).
[45] M. F. Crommie, C. P. Lutz, and D. M. Eigler, Science **265**, 218 (1993).
[46] S. V. Vonsovsky and M. I. Katsnelson, *Quantum Solid State Physics* (Springer, New York, 1989), Chap. 5.
[47] M. I. Katsnelson, I. I. Naumov, and A. V. Trefilov, Phase Transitions **49**, 143 (1994).
[48] B. G. Briner, P. Hofmann, M. Doering, H. P. Rust, E. W. Plummer, and A. M. Bradshaw, Phys. Rev. B **58**, 13931 (1998).
[49] J. Li, W.-D. Schneider, R. Berndt, O. R. Bryant, and S. Crampin, Phys. Rev. Lett. **81**, 4464 (1998).
[50] W. E. Pickett, Rev. Mod. Phys. **61**, 433 (1989).
[51] W. J. de Haas, J. de Berg, and J. van den Berg, Physica (Amsterdam) **1**, 1115 (1933–1934).
[52] J. Kondo, Prog. Theor. Phys. **32**, 337 (1964).
[53] J. Kondo, Solid State Phys. **23**, 183 (1969).
[54] A. C. Hewson, *The Kondo Problem to Heavy Fermions* (Cambridge University Press, Cambridge, 1993).
[55] D. Goldhaber-Gordon, H. Shtrikman, D. Mahalu, D. Abusch-Magder, U. Meirav, and M. A. Kastner, Nature (London) **391**, 156 (1998).
[56] S. Sasaki, S. De Franceschi, J. M. Elzerman, W. G. van der Wiel, M. Eto, and S. Tarucha, Nature (London) **405**, 764 (2000).
[57] T. W. Odom, J. L. Huang, C. L. Cheung, and C. M. Lieber, Science **290**, 1549 (2000).
[58] J. Nygard, D. H. Cobden, and P. E. Lindelof, Nature (London) **408**, 342 (2000).
[59] V. Madhavan, W. Chen, T. Jamneala, M. F. Crommie, and N. S. Wingreen, Science **280**, 567 (1998).
[60] H. C. Manoharan, C. P. Lutz, and D. M. Eigler, Nature (London) **403**, 512 (2000).
[61] J. Li, W. D. Schneider, R. Berndt, and B. Delley, Phys. Rev. Lett. **80**, 2893 (1998).
[62] W. Chen, T. Jamneala, V. Madhavan, and M. F. Crommie, Phys. Rev. B **60**, R8529 (1999).
[63] T. Jamneala, V. Madhavan, W. Chen, and M. F. Crommie, Phys. Rev. B **61**, 9990 (2000).
[64] S. H. Pan, E. W. Hudson, K. M. Lang, H. Eisaki, S. Uchida, and J. C. Davis, Nature (London) **403**, 746 (2000).
[65] U. Fano, Phys. Rev. **124**, 1866 (1961).
[66] O. Ujsaghy, J. Kroha, L. Szunyogh, and A. Zawadowski, Phys. Rev. Lett. **85**, 2557 (2000).
[67] M. Plihal and J. W. Gadzuk, Phys. Rev. B **63**, 085404 (2001).
[68] D. L. Cox, Phys. Rev. Lett. **59**, 1240 (1987).
[69] D. L. Cox and A. Zawadowski, Adv. Phys. **47**, 599 (1998).
[70] L. Kouewenhoven and L. Glazman, Phys. World **14**, 33 (2001).
[71] V. Yu. Irkhin, M. I. Katsnelson, and A. V. Trefilov, Europhys. Lett. **15**, 649 (1991); Zh. Eksp. Teor. Fiz. **105**, 1733 (1994) [JETP Lett. **78**, 936 (1994)]; Phys. Lett. A **213**, 65 (1996).
[72] A. Georges, G. Kotliar, W. Krauth, and M. Rozenberg, Rev. Mod. Phys. **68**, 13 (1996).
[73] V. Yu. Irkhin and M. I. Katsnelson, J. Phys.: Condens. Matter **4**, 9661 (1992); Phys. Rev. B **56**, 8109 (1997).
[74] M. Jarrell, Phys. Rev. B **51**, 7429 (1995).
[75] K. G. Wilson, Rev. Mod. Phys. **47**, 773 (1975); H. R. Krishnamurthy, J. W. Wilkins, and K. G. Wilson, Phys. Rev. B **21**, 1003 (1980); **21**, 1044 (1980).
[76] A. K. Zhuravlev, V. Yu. Irkhin, M. I. Katsnelson, and A. I. Lichtenstein, Phys. Rev. Lett. **93**, 236403 (2004).
[77] S. Bermon and C. K. So, Phys. Rev. Lett. **40**, 53 (1978).
[78] A. V. Balatsky, Nature (London) **403**, 717 (2000).
[79] I. Affleck and P. Simon, Phys. Rev. Lett. **86**, 2854 (2001); I. Affleck, in *Strongly Correlated Fermions and Bosons in Low-Dimensional Disordered Systems*, edited by I. V. Lerner, B. L. Altshuler, V. I. Fal'ko, and T. Giarmarchi (Kluwer, Dordrecht 2002), p. 1.
[80] T. Hänke, M. Bode, S. Krause, L. Berbil-Bautista, and R. Wiesendanger, Phys. Rev. B (to be published).